

Three-dimensional remeshed smoothed particle hydrodynamics for the simulation of isotropic turbulence

Anas Obeidat¹, Stéphane P. A. Bordas^{1,2,*}

¹*University of Luxembourg, Institute of Computational Engineering, Faculty of Science Technology and Communication*

²*Visiting Professor, Institute of Research and Development, Duy Tan University, K7/25 Quang Trung, Danang, Vietnam*

SUMMARY

We present a remeshed particle-mesh method for the simulation of three-dimensional compressible turbulent flow. The method is related to the mesh free smoothed particle hydrodynamic (SPH) method, but the present method introduces a mesh for efficient calculation of the pressure gradient, and laminar and turbulent diffusion. In addition, the mesh is used to remesh (reorganise uniformly) the particles to ensure a regular particle distribution and convergence of the method. The accuracy of the presented methodology is tested for a number of benchmark problems involving two- and three-dimensional Taylor-Green flow, thin double shear layer, and three-dimensional isotropic turbulence. Two models were implemented, direct numerical simulations, and Smagorinsky model. Taking advantage of the Lagrangian advection, and the finite difference efficiency, the method is capable of providing quality simulations while maintaining its robustness and versatility. Copyright © 2016 John Wiley & Sons, Ltd.

Received ...

KEY WORDS: remesh smoothed particle hydrodynamics, turbulent flow, three-dimensional isotropic decaying turbulence.

*Correspondence to: University of Luxembourg, Institute of Computational Engineering, Faculty of Science Technology and Communication. E-mail: stephane.bordas@uni.lu

CONTENTS

1	Introduction	3
2	Governing equations	4
2.1	Turbulence modelling	5
3	Numerical modelling	5
3.1	The hybrid remeshed SPH method	5
3.1.1	Smoothing Interpolation	5
3.1.2	Remeshing	6
3.2	The hrSPH algorithm	7
4	Verification for the hrSPH method for viscous flow	9
4.1	Two-Dimensional Taylor-Green flow	10
4.2	Thin double shear layer	13
4.3	Three-dimensional Taylor-Green flow	15
4.4	Three-dimensional isotropic turbulence	20
5	Conclusion	24
6	Acknowledgements	24

1. INTRODUCTION

The Smoothed Particle Hydrodynamics (SPH) method was introduced independently by Gingold and Monaghan [2], and by Lucy [4], with the aim to simulate astrophysical problems. Over the years SPH has been extended and applied in many areas. Stam and Fiume [18] first used SPH to simulate fire. Müller et al. [23] developed an SPH method which can be applied on real-time fluid simulation. The SPH method was also extended in free surface flows problems [15], and low-Reynolds number viscous flows [10, 19, 32], Cummins et al. [12] extended SPH to simulate incompressible fluids, followed by Shao et al. [35] who propose an SPH simulation for Newtonian and non-Newtonian flows with a free surface. Cleary and Monaghan [38] extended SPH to heat transfer simulation, and finally the method was developed for multi-phase flows simulation by Morris [31].

Turbulence modelling with SPH is a rather new field of research. Monaghan [16] introduced a Lagrangian-averaged Navier-Stokes turbulence model modifying the original SPH method for the simulation of two-dimensional turbulence. The method is computationally inefficient due to the reduced time step compared to the spectral method one [13], but the simulated energy spectrum and velocity profiles were found to be in good agreement with the results obtained using spectral methods.

Three SPH turbulence models were introduced by Violeau and Issa [8], two algebraic models, and one based on the Reynolds stress model. Two-dimensional open channel turbulent flow and two-dimensional collapsing water column cases were simulated, the kinetic energy, dissipation rate and eddy viscosity results were in good agreement with Monaghan [16] results, but the method may not be competitive in comparison with grid-based method, due to the small time step required resulting a large computational cost.

Dalrymple and Rogers [1] used a large eddy simulation (LES) turbulence model to simulate two-dimensional breaking waves with SPH. Robinson and Monaghan [24] studied how SPH performs in a direct numerical simulation (DNS) of decaying turbulence in a two-dimensional no-slip wall-bounded domain. They showed that the original SPH method can reproduce the energy cascade, which filled to an end state of a large monopole vortex that filled the domain, but their work was limited to two-dimensional cases.

Ellero et al. [22] and Shi [41] studied isotropic homogeneous turbulence cases with high Mach number and showed that SPH in its original form has an effective implicit viscosity. Finally Adami [33] proposed a new algorithm combining the homogenisation of the particle configuration by a background pressure which reduces the artificial numerical dissipation.

In this work we present a hybrid remeshed smoothed particle hydrodynamics method (hrSPH) for the simulation of three-dimensional turbulent flows. Rather than simplifying the framework and solve the system of equations solely on the grid, we combine an Eulerian mesh with Lagrangian particles to use the advantages of both schemes. We want to keep the free of the convection Courant Friedrichs Lewy (CFL) condition that the classical SPH method enjoys, whilst to take advantage of the computational efficiency to compute the derivatives on the grid, which is computationally cheaper than the nearest neighbour search of mesh free particle methods. The hrSPH also shares the adaptive character of SPH. The hrSPH framework is the first step toward a wider vision, in which the Lagrangian part (i.e. the particles) will play an important rule when a complex geometry is needed. After all, it combines the abilities to apply Particle-Particle interactions to a part of the PDEs and Finite Differences to the other part.

The method is based on the remeshed smoothed particle method introduced by Chaniotis et al. [20] and Chatelain et al. [26]. The presented method differs from that the one of Chaniotis, as we take advantage of both the Lagrangian properties of the SPH along with the efficiency of Finite Difference scheme in which we interpolate the particles and compute the governing equations on the right hand side, rather than performing Particle-Particle interactions. We furthermore extend the framework of Chatelain et al. [26] in order to solve the full set of the Navier-Stokes equations. Subsequently, we add a the subgrid model to the system of equations.

The particles are remeshed (uniformly reinitialised) onto uniform grid using a third order interpolation scheme to overcome the clustering or distortion of particles.

The mass and the impulse of the particles are interpolated onto the mesh, where the moments (mass, momentum, angular momentum, etc.) rate of change is computed. These are used to update the velocity and the position of the particles.

Direct numerical simulations (DNS), along with Smagorinsky [17] model are applied in this study. Details of the governing equations are presented in section 3, and the hrSPH method is explained in section 4, and finally the two- and three-dimensional results are presented in section 5.

2. GOVERNING EQUATIONS

The compressible flow is governed by the Navier-Stokes equations describing conservation of mass

$$\frac{D\rho}{Dt} = -\rho \frac{\partial u_i}{\partial x_i} \quad (1)$$

and conservation of momentum,

$$\rho \frac{Du_i}{Dt} = \frac{\partial p}{\partial x_i} + \frac{\partial \tau_{ij}}{\partial x_j} + \frac{\partial \tau_{ij}^{sgs}}{\partial x_j} \quad (2)$$

where

$$\tau_{ij} = \mu \left(\frac{\partial u_i}{\partial x_j} + \frac{\partial u_j}{\partial x_i} - \frac{2}{3} \delta_{ij} \frac{\partial u_k}{\partial x_k} \right), \quad (3)$$

where $\frac{D\phi}{Dt} = \frac{\partial \phi}{\partial t} + (u \cdot \nabla) (\phi)$ denotes the material derivative, u_i is the velocity, p is the pressure, ρ is the density, τ_{ij} is the shear stress, μ is the dynamic viscosity, δ_{ij} is the Kronecker delta, and τ_{sgs} is the sub-grid stress tensor, which is zero in case of direct numerical simulation.

In the presented work the flow is uniquely described by the Reynolds number $Re = U\rho_0 L/\mu$, and the Mach number $Ma = U/c$. L is the characteristic length, ρ_0 is the reference density, U is the reference velocity, and c is the speed of sound.

To close the system (Eqs. (1-2)), the following equation of state is used,

$$p = \rho c^2 \quad (4)$$

2.1. Turbulence modelling

Direct numerical simulations are generally limited to low Reynolds number flow due to the available computational resources. In the present work we model the turbulent sub-grid stresses using the standard Smagorinsky model [17], defined as

$$\tau_{ij}^{sgs} = \rho (C_s \Delta)^2 \sqrt{2S_{ij}S_{ij}} \widehat{S}_{ij} \quad (5)$$

with

$$\Delta = h, \quad (6)$$

where C_s is a non dimensional constant for which values ranging from 0.1 to 0.24 have been suggested in literature [34], Δ is the model length scale which is proportional to the the grid spacing Eq. (6), h are the mesh spacing, $\widehat{S}_{ij} = \frac{1}{2} \left(\frac{\partial u_i}{\partial x_j} + \frac{\partial u_j}{\partial x_i} \right) - \frac{2}{3} \frac{\partial u_k}{\partial x_k} \delta_{ij}$ is the the filtered strain tensor, and $(C_s \Delta)^2 \sqrt{2S_{ij}S_{ij}}$ is the norm of the filtered strain tensor, where $S_{ij} = \frac{1}{2} \left(\frac{\partial u_i}{\partial x_j} + \frac{\partial u_j}{\partial x_i} \right)$

3. NUMERICAL MODELLING

3.1. The hybrid remeshed SPH method

The basic idea of the hybrid remeshed smooth particle method (hrSPH) is to discretise the governing equations using Lagrangian particles carrying mass and impulse; the hybrid remeshed SPH method computes the right-hand side (RHS) of the governing equations by interpolating the mass and impulse of the particle onto a regular mesh, and from these, the flow density and velocity fields are obtained on the mesh nodes. These in turn allow for efficient calculation of the RHS using high order finite differences.

The used interpolating technique is explained in the following part.

3.1.1. Smoothing Interpolation

The particle-to-mesh and mesh-to-particle interpolation is obtained using moment conserving interpolation. The interpolation was introduced to minimise the error that ordinary (not continuous everywhere) interpolations produce, through a moments-conserving interpolation (conservation of mass, momentum, angular momentum, etc.) [39, 28, 9]. However in mesh-to-particle interpolation, conservation of moments is generally not possible due to the non-uniform spacing of the target particles, though the interpolation error decreases as a power of the mesh spacing h . This power is called the order of convergence of the interpolation scheme.

The strengths (characteristics) of the particles (mass, and impulse) read:

$$w_p = \begin{pmatrix} m_p \\ m_p u_p \end{pmatrix}, \quad (7)$$

where, u_p is the three velocity component u, v, w , and m_p is the mass of the particle.

Fig. 1 shows 2-dimensional particle-to-mesh interpolation, where the strength of the particle is interpolated to the mesh using high order kernel as following:

$$\omega(x_m) = \sum_{p=1}^N \omega_p W(x_m - x_p, h), \quad (8)$$

where N is the number of particles, h is the mesh spacing, W is the high order kernel, ω_p is the strength of the particles, x_m is the position of mesh node m , and x_p is the position of particle p .

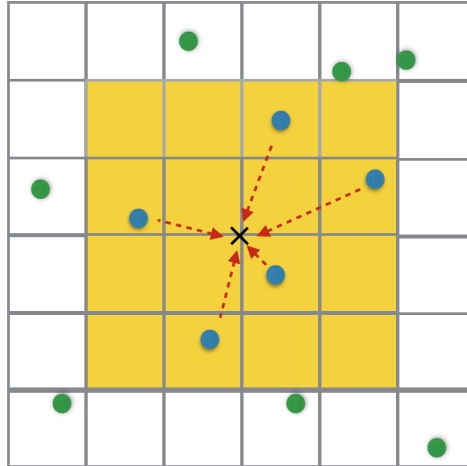


Figure 1. Schematic representation of particle-to-mesh interpolation in 2D using an interpolation function with support region $\pm 2h$ (shaded in yellow). Blue particles are within the support region of the centre node (black) and hence assigned onto it. Green particles which lie outside the support region are not considered.

The smoothing interpolation is continuous everywhere in the interpolation stencil, and provide moment conserving interpolation. The M^4 introduced by [14] interpolate the strength of the particles to the mesh, the strengths are redistributed onto the surrounding mesh nodes as follows

$$M^4(x, h) = \begin{cases} 1 - \frac{5s^2}{2} + \frac{3s^3}{2} & 0 \leq s < 1, \quad s = \frac{|x|}{h} \\ \frac{(1-s)(2-s)^2}{2} & 1 \leq s < 2, \\ 0 & s \geq 2, \end{cases} \quad (9)$$

where $|x|$ is distance of the particle to the mesh.

This M^4 kernel has a four-point support with an error of $O(h^3)$, and the stencil of the discrete interpolation operator based on M^4 consists of 64 grid points.

The differential operator for the momentum equation are computed on the mesh, taking advantage of finite difference efficiency rather than using the particle-particle interaction. To maintain the Lagrangian advantages of the hrSPH, advection is taking part on the particles, by interpolating the rate-of-change in momentum to the particles (mesh-particle interpolation), which is used to integrate the velocity and position of the particles forward in time.

We note the mesh controls the adaptivity and provides support for the fast evaluation of the pressure and stress tensor terms, the hrSPH mainly keeps the linear stability unconditional. The non-linear stability condition requires that particles trajectories do not cross [29]

$$\Delta t \leq C \|\nabla u\|_{\infty}^{-1}, \quad (10)$$

where Δt is the time step, and C is the no linear Courant Friedrichs Lew (CFL) condition.

3.1.2. Remeshing

In the SPH method particles may cluster in one area of the computational domain and spread apart in another, as a result of the strain of the flow. When this occurs, the system loses the ability to recover continuous velocity and density fields.

When the distortion of the particle distribution occurs, the particle-mesh interpolation function is unable to ensure the continuity of the system, resulting in the inaccurate representation of the diffusion effect along with the pressure gradient (rate-of-change of momentum). To abrogate this

problem, Chaniotis et al. [20] introduced the re-meshed smooth particle hydrodynamics method in which the position of the particles is periodically reinitialised to a uniform grid and the old particles properties are interpolated to the new ones. This interpolation has been implemented in several methods including particle methods [27, 30, 28].

By remeshing the particles using the high order interpolation kernel the following is accomplished:

- We retain the Lagrangian characteristic and the stability of the particle method. This gives us a large amount of control over the accuracy, as it leads to a more accurate computation of the derivatives compared to the classical particle-particle interaction (classical SPH).
- We decrease the computational costs thanks to:
 1. The exploitation of the regularity of the particles.
 2. Avoiding the costly nearest neighbour search. SPH method requires nearest neighbour searches for each particle to evaluate derivatives such as the pressure gradient. This adds to the computational costs of the classical SPH. We also remesh the particles and solve the right hand side of the equations on the grid. This increases the computational efficiency as nearest neighbours do not have to be found and the speed of Finite Difference schemes is utilised. The cost of remeshing each time step is around 10% of the total costs [20] which is a small price compared to the total cost that the SPH required, along to the advantage of ensuring that the particles are always in-space, resulting an accurate approximation of the flow strain.
 3. The interpolation of the particle's characteristics on a uniform grid grants the method an increased computational efficiency to compute the derivatives using Finite Differences.
- Remeshing ensures that particles do not get too close to each other. This is an advantage as the pressure force in the momentum equation proportional to the derivative of the kernel, which in the case of M^4 is reduced to zero when the distance between the particles is small. In this case the pressure force becomes attractive resulting in significant errors in the classical SPH method [20].

The remeshing frequency in our framework can vary depending on the strain of the flow and the size of the time step. If the particles maintain their uniform distribution, as in the case of uniform flow fields without circulations and low Reynolds number (Re), remeshing only needs to be applied once per ten time steps, or even less frequent. In case of turbulent flows in which the flows recirculate however, remeshing is performed for every time step [20]. In the test cases in this framework we perform remeshing every time step, unless stated otherwise.

The accuracy of the method comes with a minimal additional computational cost while maintaining the adaptive character of the method. The implementation of high-order remeshing schemes improves the accuracy of hrSPH and additionally increases the computational efficiency of the algorithm.

The remeshing algorithm with finite support may result in numerical errors, as it may introduce substantial numerical diffusion. However, Koumoutsakos [28] and Chaniotis et al. [20] have shown that the introduced dissipation by remeshing and the errors of the computed gradients, induced by particle distortion, are proportional. These gradients remain substantially small if remeshing is performed at each time step. As discussed by Koumoutsakos [28] finally, remeshing acts like a subgrid scale and has a negligible effect on the accuracys

3.2. The hrSPH algorithm

Our method is divided into three parts:

1. Computing the rate of change

- (a) Particle-mesh interpolation of the mass and impulse of the particle.

$$m(x_m) = \sum_{p=1}^N m_p W(x_m - x_p, h), \quad (11)$$

$$m(x_m)u(x_m) = \sum_{p=1}^N m_p u_p W(x_m - x_p, h) \quad (12)$$

where N is the number of particles, h is the mesh spacing, W is the high order kernel, u is the three velocity component u, v, w , and m_p is the mass of the particle, x_m is the position of mesh node m , and x_p is the position of particle p .

- (b) On the grid, obtain the velocity from the interpolated impulse

$$u(x_m) = \frac{m(x_m)u(x_m)}{m(x_m)} \quad (13)$$

- (c) On the grid, compute the fluid density from the interpolated mass and the pressure from the equation of state Eq. (4).

$$\rho(x_m) = \frac{m(x_m)}{h^3} \quad (14)$$

- (d) On the grid, compute the rate-of-change of the fluid momentum on the mesh (Δu_m) using finite-differences.

- (e) The rate-of-change of momentum is interpolated from the grid to the particles (Δu_p), Fig. 2.

$$\Delta u(x_p) = \sum_{m=1}^N \Delta u_m W(x_m - x_p, h) \quad (15)$$

2. Updating the particles

This part takes place on the set of particles, where the interpolated rate of change in velocity is used to update the velocity and position of the particles.

$$\vec{u}_p^{t+1} = \vec{u}_p^t + \Delta \vec{u}_p * \Delta t \quad (16)$$

$$\vec{x}_p^{t+1} = \vec{x}_p^t + \vec{u}_p * \Delta t \quad (17)$$

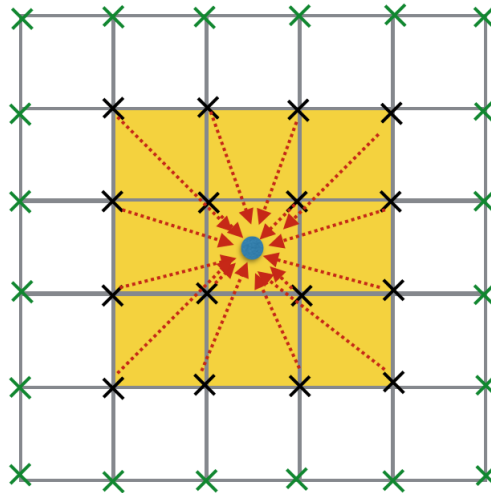


Figure 2. Schematic representation of mesh-to particle interpolation in 2D using an interpolation function with support region $\pm 2h$ (shaded in yellow). the blue particle and mesh nodes (black) are within the support region of the centre particle and hence assigned onto it. Green mesh and nodes lying outside the support and are not considered.

3. Remeshing the particles:

In case of distortion and particle clustering (high CFL number, high gradients), interpolate the strengths of the particles to the mesh via M^4 interpolation function, generate a new set of the particles, interpolate the strengths back to the new set of particles.

For clarity an pseudo-code of the hrSPH algorithm follows,

Initialisation: Create particles carrying the initial mass m_p , and impulse $m_p u_p$;

while $t < endTime$ **do**

On the particles:

for $p=1$ to N **do**

 | Interpolate the particle impulse and mass to the grid Eq. (11, 12).

end

On the grid:

for $p=1$ to N **do**

 | Obtain the velocity from the interpolated impulse Eq. (13);

 | Obtain the density from the interpolated mass Eq. (14);

 | Obtain the pressure from the equation of state Eq. (4);

Right hand side computation:

 | Using finite-difference, compute the rate-of-change of the fluid momentum Eq. (2);

end

for $p=1$ to N **do**

 | Interpolate the the change of momentum to the particles Eq. (15).

end

On the particles:

for $p=1$ to N **do**

 | Update the velocity and position of the particles Eq. (16, 17).

end

if *Remeshing* = *true* **then**

 | Do remeshing;

end

end

Algorithm 1: The hrSPH algorithm

Solving the continuity equation Eq. (1) is not consistent with the system, rather the mass of the particles is updated via the M^4 function. This sequence is repeated in a third-order Runge-Kutta scheme [3] The pressure gradient is solved with a second order central difference scheme, while diffusion is computed using a second order central difference scheme.

We want to note that the number of the particles is equivalent to the number of the grid points in all benchmarks in section (4), unless the number of the particles is stated explicitly. As mentioned before, remeshing is furthermore performed at every time step, unless stated otherwise.

4. VERIFICATION FOR THE HRSPH METHOD FOR VISCOUS FLOW

To verify the method, we perform a series of benchmarks, including: two- and three-dimensional Taylor-Green flow [11], thin double shear layer [21], and three-dimensional isotropic turbulence. In this manuscript the flow is characterised by the dimensionless Mach number Ma and the Reynolds number Re , which allow the reader to reproduce any of the benchmarks. The characteristic length scales L are the computational domain unless otherwise is stated, and the velocity u is normalised by either the maximum velocity or the reference velocity.

4.1. Two-Dimensional Taylor-Green flow

As a first test of the hrSPH method, we perform a simulation of the 2D incompressible Taylor-Green flow. Taylor-Green is a periodic flow of decaying vortices in the x - y plane as follows,

$$u(x, y, t) = -Ue^{bt} \cos\left(\frac{2\pi x}{L}\right) \sin\left(\frac{2\pi y}{L}\right) \quad (18)$$

$$v(x, y, t) = Ue^{bt} \sin\left(\frac{2\pi x}{L}\right) \cos\left(\frac{2\pi y}{L}\right) \quad (19)$$

$$p(x, y, t) = p_0 - \frac{U^2}{4} e^{bt} \left[\cos\left(\frac{4\pi x}{L}\right) + \cos\left(\frac{4\pi y}{L}\right) \right], \quad (20)$$

where $b = \frac{-8\pi^2}{Re}$, $Re = \rho_0 U L / \mu$ is the Reynolds number, L is the characteristic length of the system, ρ_0 is the reference density, μ is the viscosity. To approximate the incompressible reference solution, we choose a Mach number Ma is equal to 0.1, and the pressure reference is $p_0 = \frac{1}{M^2}$. The computational domain is $[L \times L]$ with periodic boundary conditions. We perform simulations for Reynolds numbers in the range $(10^0 - 10^3)$ to validate the accuracy of the method with the viscous effect (dominant, intermediate and minimal). The third order Runge-Kutta scheme is used throughout with a constant time step.

The flow maximum velocity decay behaviour with $Re = 10^0$ calculated using hrSPH with resolution of $[64 \times 64]$ is presented in Fig. 3 which shows a good agreement with the incompressible exact solution $U_{ex} = Ue^{bt}$.

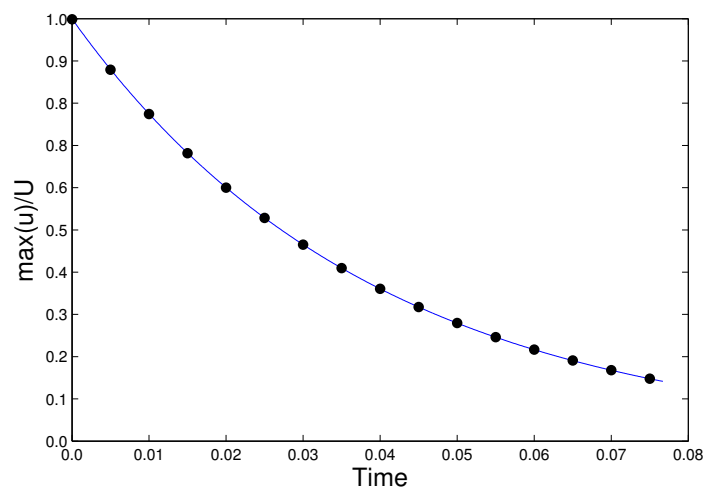


Figure 3. The maximum normalised velocity decay profile with $Re = 10^0$. Comparison of the hrSPH solution (-) with the exact incompressible solution(\bullet). The hrSPH solutions shows a good agreement with the the incompressible exact solution $U_{ex} = Ue^{bt}$.

To test the accuracy of the method at higher Reynolds numbers we perform simulations at $Re = 10^2$. The predicted velocity decay shown in Fig. 4 is found in excellent agreement with the exact solution.

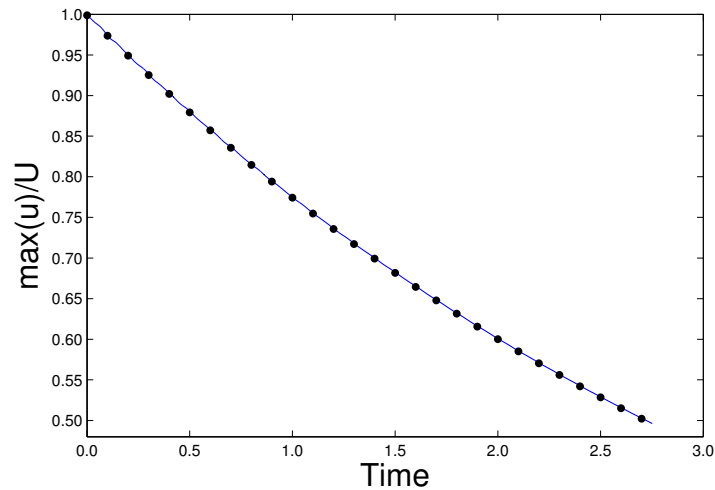


Figure 4. The maximum normalised velocity decay profile with $Re = 10^2$. Comparison of the hrSPH solution (-) with the exact incompressible solution (\bullet). The hrSPH solutions shows a good agreement with the the incompressible exact solution $U_{ex} = Ue^{bt}$.

For the error analysis of the hrSPH simulation, the relative error (L_∞) is used

$$L_\infty(t) = \left| \frac{u(t) - U_{ex}(t)}{U_{ex}(t)} \right|, \quad (21)$$

where, $u(t)$ is the maximum velocity magnitude of the hrSPH simulation at time t , and $U_{ex}(t)$ denotes the maximum velocity magnitude of the exact solution at time t .

The relative error L_∞ for the hrSPH method calculation is between 0.5% and 1.4% for $Re = 10^2$ Fig. 5, which is twice as accurate then previously reported for SPH simulations [33, 20].

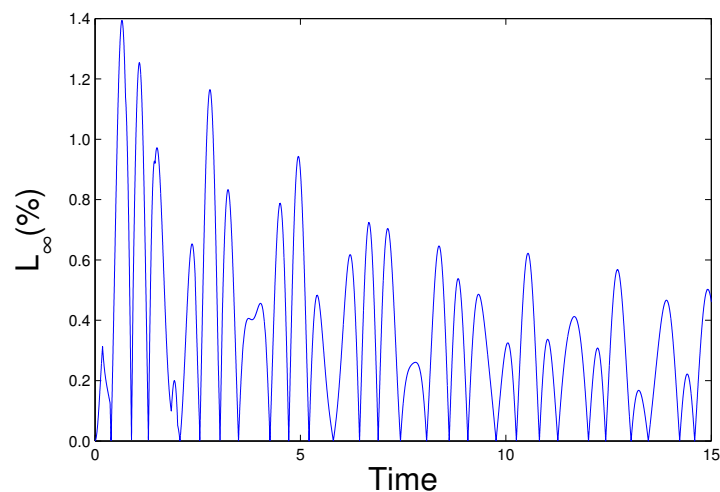


Figure 5. The relative error of the maximum velocity for the 2D Taylor-Green flow at $Re = 10^2$ using the hrSPH method with resolution of $[64 \times 64]$. The relative error L_∞ for the hrSPH method calculation is between 0.5% and 1.4% for $Re = 10^2$

The hrSPH relative error increases as the Reynolds number increases for a fixed grid resolution, with less numerical dissipation which is a plus advantage for the hrSPH method.

The maximum of the relative error $\max(L_\infty)$ shown in Fig. 6, for a 64×64 resolution is less than 2% for Re in the range considered $1 - 10^3$.

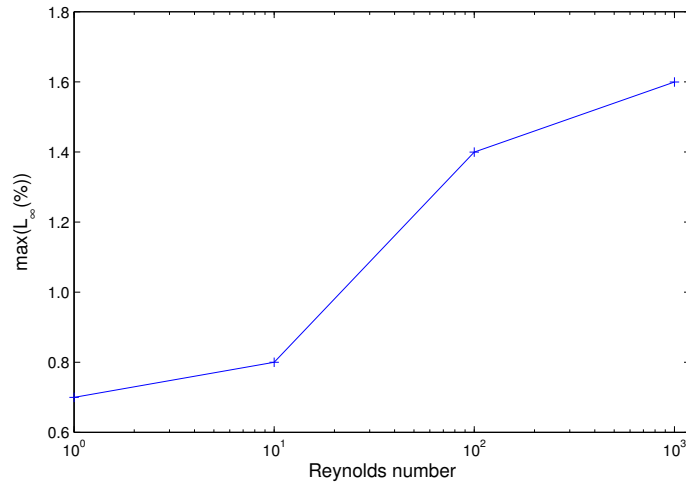


Figure 6. $\max(L_\infty)$ error of the hrSPH simulations of the 2D Taylor-Green flow for different Reynolds number with a fixed grid resolution $[64 \times 64]$. The maximum of the relative error $\max(L_\infty)$ is less than 2% for Re in the range considered $1 - 10^3$.

Finally we tested the convergence rate of the relative error L_∞ for a spatial grid refinement. The profile of the maximum relative error $\max(L_\infty)$ of the hrSPH simulation with different resolution $[16 \times 16, 32 \times 32, 64 \times 64, 128 \times 128, \text{ and } 256 \times 256]$ is presented in Fig. 7

The hrSPH exhibits a third order convergence in space, with third order diffusion and pressure gradient, which is consistent with the order of the M^4 interpolation function as represented in Fig. 7.

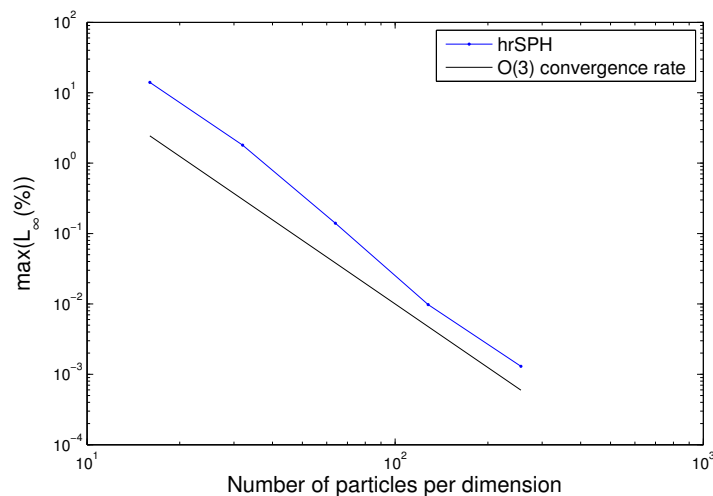


Figure 7. $\max(L_\infty)$ error of the hrSPH simulations for the Taylor-Green flow with different resolutions with $Re = 100(\cdot)$, along with the third order convergence rate. The hrSPH exhibits a third order convergence in space, which is consistent with the order of the M^4 interpolation function.

4.2. Thin double shear layer

To illustrate the performance of the hrSPH method on under resolved flow, we simulated the evolution of a thin double shear layer. The thin double shear layer, which is often considered to be too difficult to simulate due to the produced small scales. The main challenge of this problem as showed by Brown and Minion [21], occurs when the method is producing the spurious structures, in the case when the flow is sufficiently under-resolved. Brown and Minion [21] tested several numerical schemes, and showed that given a sufficient resolution (256×256) all the numerical schemes provided a reasonably accurate solutions. But given a coarser mesh (128×128) the methods generate a non physical spurious vortex in the shear layer between the two vortices, with an early oscillations at $t = 1.0$.

Drikakis and Smolarkiewicz [6] studied the spurious structure, aiming to understand the numerical mechanism behind it. They indicated that the generation of the spurious structure depends on the choice of the advective scheme.

The computational domain is a unit square with periodic boundary conditions. The flow velocity $\mathbf{u} = (u, v)$ is initially consists of a horizontal shear layer of a finite thickness as

$$u(x, y) = \tanh(80 \times \min(y - 0.25, 0.75 - y)) \quad (22)$$

$$v(x, y) = \delta \sin(2\pi(x + 0.25)), \quad (23)$$

In the simulation we set $\delta = 0.05$, Reynolds number $Re = 10^4$, and Mach number $Ma = 0.1$, initially we start with a uniform pressure and density. Fig. 9 shows the evolution of the vorticity for three different mesh resolutions; a fine one with 400×400 , a 200×200 , and a coarser one with 100×100 . We note that using the hrSPH method, with a relatively low resolutions we are able to overcome the development of the spurious vortex compared to previous studies [7] cf. Fig. 8.

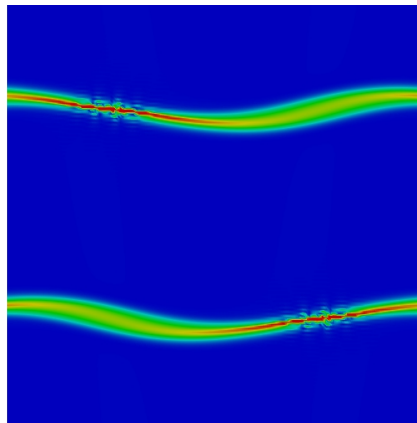


Figure 8. The development of a spurious vortex for the lower resolutions 256×256

However with the coarse 100×100 mesh the hrSPH method produces the spurious structure and the simulation failed, which agrees with the previous studies in [21].

The vorticity evolution for both resolutions 400×400 , and 200×200 is presented in Fig. 9, both cases were able to avoid the spurious structure.

With Reynolds number $Re = 3 \times 10^3$ a resolution of 100×100 the hrSPH is able to simulate without producing the spurious structure. At time $t \approx 4$ we notice that oscillations are produced, as mentioned by Minion [21], however this problem occurred after a long simulation time, as shown in Fig. 10.

As the hrSPH enjoys the benefits of a Lagrangian advection, the method is able to provide accurate results for the thin double shear layer with a lower mesh resolution meshes compared to previous studies [21, 6, 7].

Finally the calculated maximum error of the relative effective viscosity [5] $\mu_{eff}(t) = \frac{\epsilon(t)}{\epsilon(t)}$ to the physical viscosity μ , where ϵ is the dissipation rate Eq. (24), and ϵ is the enstrophy Eq. (25).

$$\epsilon = \frac{dE_k}{dt} \quad (24)$$

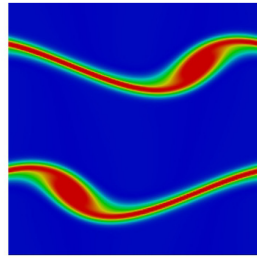
$$\epsilon = \int_{\Omega} \frac{\omega \cdot \omega}{2} d\Omega, \quad (25)$$

where E_k is the kinetic energy

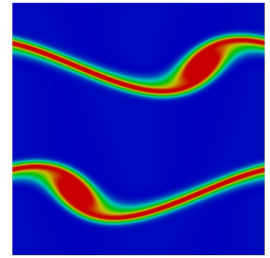
$$E_k = \int_{\Omega} \rho \frac{u \cdot u}{2} d\Omega, \quad (26)$$

and ω is the vorticity, and Ω is the computational domain.

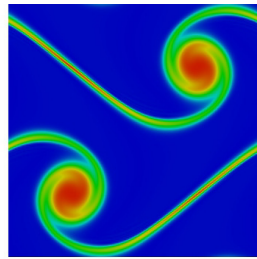
For the thin double shear layer flow with $Re = 10^4$ and resolution of 200×200 at $t = 1$, the maximum error of the relative effective viscosity is equal to 2%.



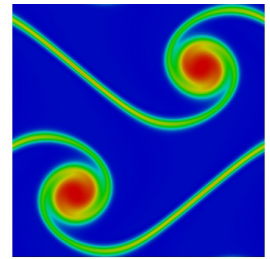
(a) time = 0.6



(b) time = 0.6



(c) time = 1.0



(d) time = 1.0

Figure 9. Vorticity magnitude of the thin double shear layer simulation with $Re = 10^4$. Left column using 200×200 particles, and right column using 400×400 particles. The hrSPH is able to avoid the development of the spurious structure with a lower grid resolution compared to [7].

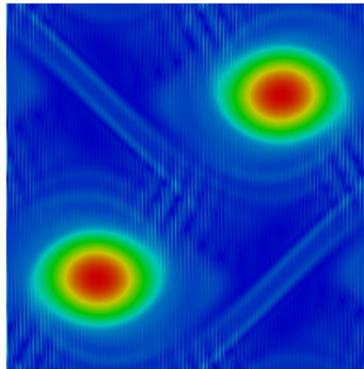


Figure 10. The produced oscillation for the thin double shear layer using the hrSPH using a coarse 100×100 mesh. The hrSPH is able to avoid the development of the spurious structure, however oscillations are produced at time $t \approx 4$.

4.3. Three-dimensional Taylor-Green flow

This benchmark considers direct numerical simulation (DNS) with hrSPH method, three-dimensional Taylor-Green is a periodic flow of decaying vortices in the $x - y - z$ plane, with the following initial conditions,

$$u(x, y, z) = U \sin\left(\frac{2\pi x}{L}\right) \cos\left(\frac{2\pi y}{L}\right) \cos\left(\frac{2\pi z}{L}\right) \quad (27)$$

$$v(x, y, z) = -U \cos\left(\frac{2\pi x}{L}\right) \sin\left(\frac{2\pi y}{L}\right) \cos\left(\frac{2\pi z}{L}\right) \quad (28)$$

$$w(x, y, z) = 0 \quad (29)$$

$$p(x, y, z) = p_0 + \frac{\rho_0 U^2}{16} \left(\cos\left(\frac{2\pi x}{L}\right) + \cos\left(\frac{2\pi y}{L}\right) \right) \left(\cos\left(\frac{2\pi z}{L}\right) + 2 \right), \quad (30)$$

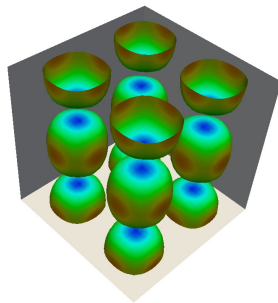
where, U_0 is the reference velocity, the Mach number $Ma = 0.1$, L is the respective length, and p_0 is the reference pressure, which is determined from the reference density ρ_0 by the equation of state Eq. (4).

The aim of this test case is to test the accuracy of hrSPH for three-dimensional viscous flow with Reynolds number $Re = 1600$, using direct numerical simulation. The flow is confined in a cube with periodic boundary conditions defined as $0 \leq x, y, z \leq 2\pi$. The computational meshes are regular cartesian grids of 64^3 , 128^3 , 256^3 resulting in $\Delta x = 0.01, 0.05, 0.025$. The third order Runge-Kutta is used for time interpolation. Fig. 11, represents the isosurface of the vorticity magnitude at different times. The evolution of the kinetic energy over time is presented in Fig. 12 (a), we observe that the hrSPH method is capable to capture the basic dynamic flows for different grid resolutions and is in a good agreement with the reference solution [36]. The change in the kinetic energy over time for the three grid resolutions is insignificant, however the close up is shown in Fig. 12 (b), shows that the coarser grid contains less energy than the finer one, and the energy decays faster as time evolve.

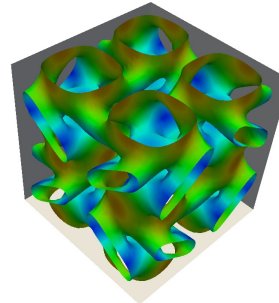
At early time steps as the vortices begin to evolve and maintain their shape, this phase lasts approximately until $t = 7$ where the smooth structures begins to suffer changes in their structure as the flow becomes turbulent, at $t = 9$ the coherent structure breaks down.

Fig. 13 depicts the evolution of the dissipation rate (ϵ) Eq. (24), and the enstrophy (ε) Eq. (25). Fig. 13(a) shows the time history of the enstrophy, it is clear that there is a large change in the peak dissipation rate for the coarser grid ($\Delta x = 0.01$), this peak is improved by increasing the grid resolution until we reach a good agreement with the reference solution at grid resolution $\Delta x = 0.025$. The dissipation rate is represented in Fig. 13(b), we examine a large difference in the dissipation peak at $t = 9$ where the coarser grid fails to estimate the correct dissipation peak. The finer grid, with $\Delta x = 0.025$, is consistent with the reference solution [37]. We calculated the error of the relative effective viscosity $\mu_{eff}(t) = \epsilon(t)/\varepsilon(t)$ to the physical viscosity. The maximum error in the relative effective viscosity is about 2% for the hrSPH method.

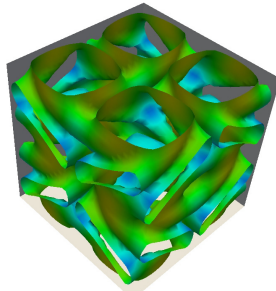
To finally test the effect of the remeshing frequency, we run the same test case at $Re = 1600$ with $\Delta x = 0.05$, whilst decreasing the time step by a factor of two ($\Delta t = \Delta t/2$) and keeping the remeshing frequency the same, we used the solution of the kinetic energy evolution with $\Delta x = 0.05$ presented in Fig. 12 (a) as a reference solution to calculate the relative error $L_\infty(\%)$. The reason is to check if our computation is well converged in time resolution. The results in Fig. 14(b) show that no effect on the solution and the relative error $L_\infty(\%)$ is approximately 0%. This leads us to conclude that any changes in the solution will be a result of changing the remeshing frequency. We thus also performed two test cases in which the remeshing frequency is increased by a factor of two and four respectively, while decreasing the time step with a factor of two and four as well. The results in Fig. 14(a), (b) show that the remeshing frequency affects the results when the flow contains a substantial kinetic energy and small scales. The relative error of the kinetic energy is approximately 2% when remeshing is performed at every time step and approximately 4.5% if remeshing is performed once per four time steps. This can be explained based on the fact that remeshing allow the system to regain it's regularity as it ensures the particles' uniform distribution, even when flows with a large Reynolds number are considered. As the kinetic energy decreases as a function of time, the relative error reduces to well below 1%.



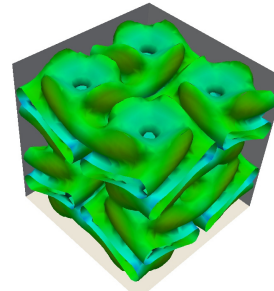
(a) time = 0



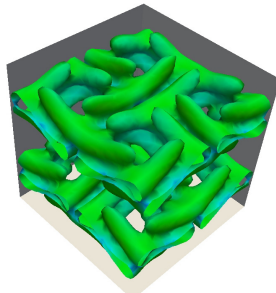
(b) time = 2



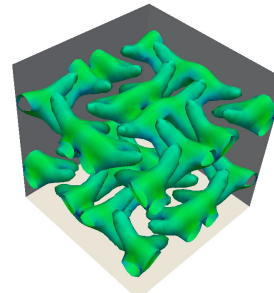
(c) time = 4



(d) time = 8



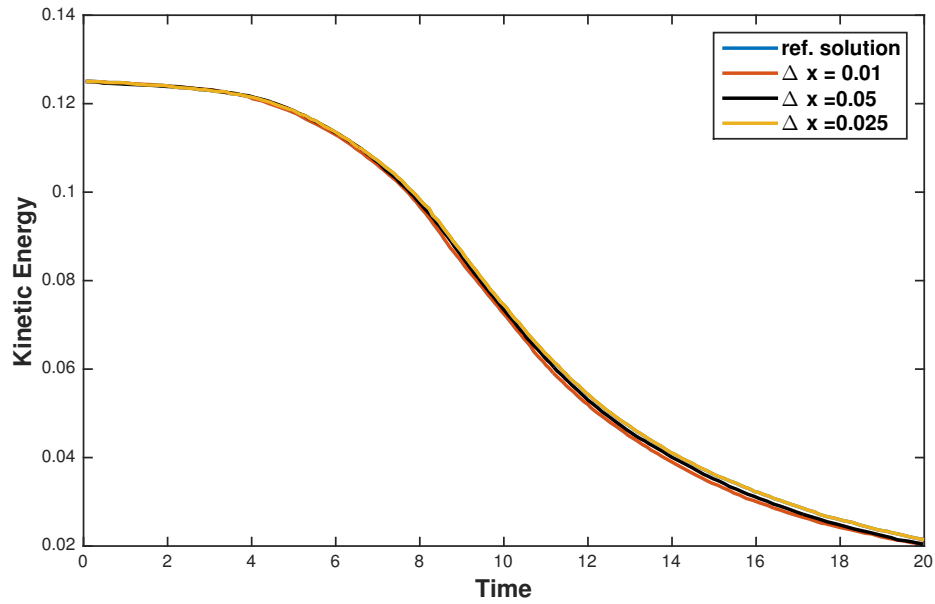
(e) time = 12



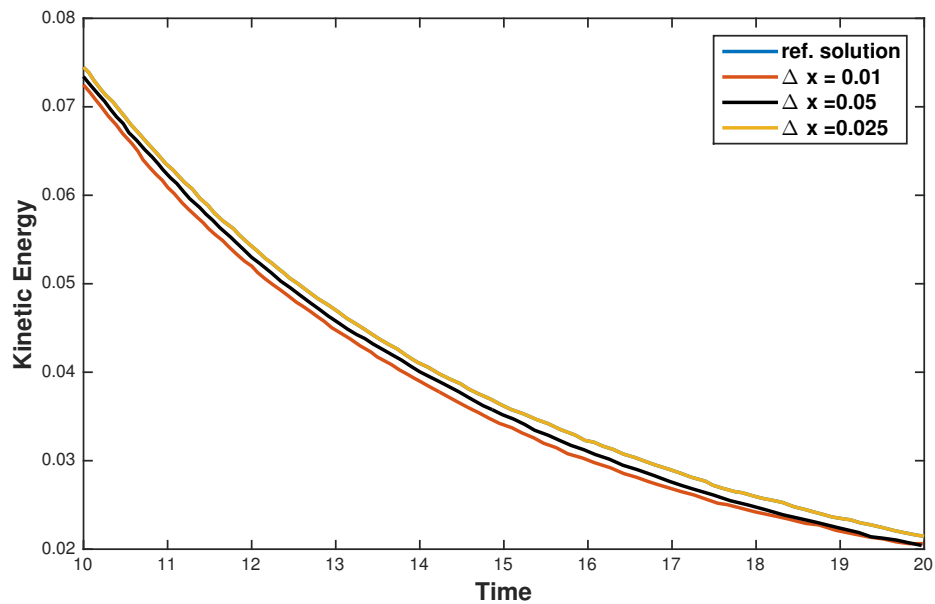
(f) time = 16

Velocity magnitude



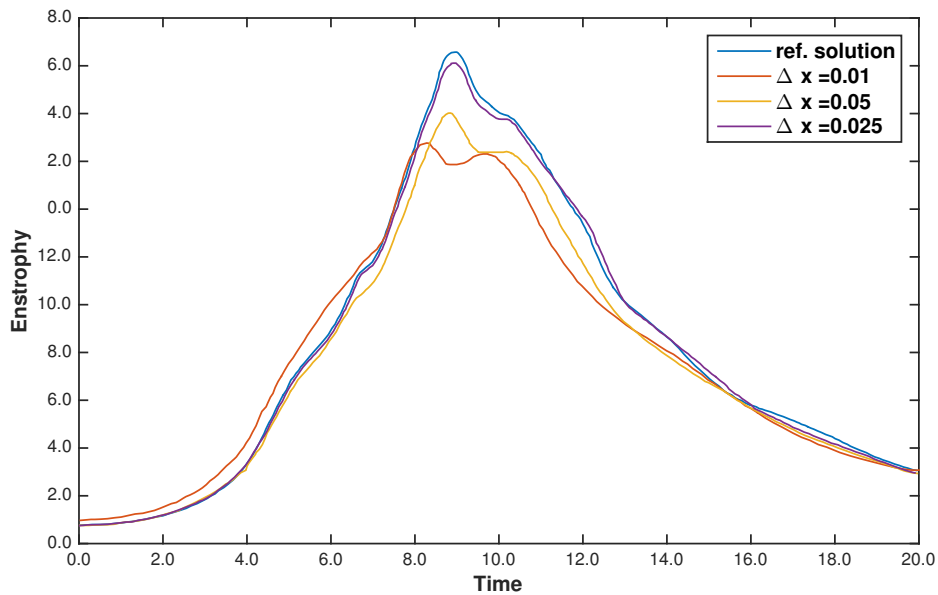


(a) Complete simulation.

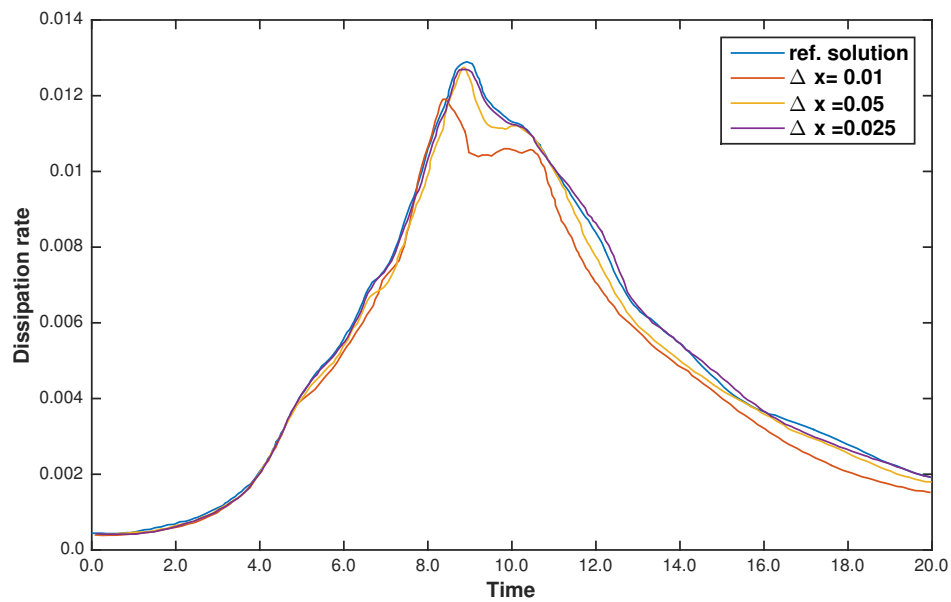


(b) Part of the simulation 10;time;20.

Figure 12. Evolution of the kinetic energy for the 3D Taylor-Green simulation, $Re = 1600$, using the hrSPH method, with different resolution along with the reference solution. In (a), we observe that the hrSPH method is capable to capture the basic dynamic flows for different grid resolutions and is in a good agreement with the reference solution. The close up in (b), shows that the coarser grid contains less energy than the finer one, and the energy decays faster as time evolve.



(a)



(b)

Figure 13. Evolution of enstrophy (a), and dissipation rate (b) for the simulation of the 3D Taylor-Green at $Re = 1600$ with different resolution using the hrSPH method. In (a) there is a large change in the peak dissipation rate for the coarser grid, this peak is improved by increasing the grid resolution until we reach a good agreement with the reference solution. In (b) we examine a large difference in the dissipation peak at $t = 9$ where the coarser grid fails to estimate the correct dissipation peak. The finer grid is consistent with the reference solution.

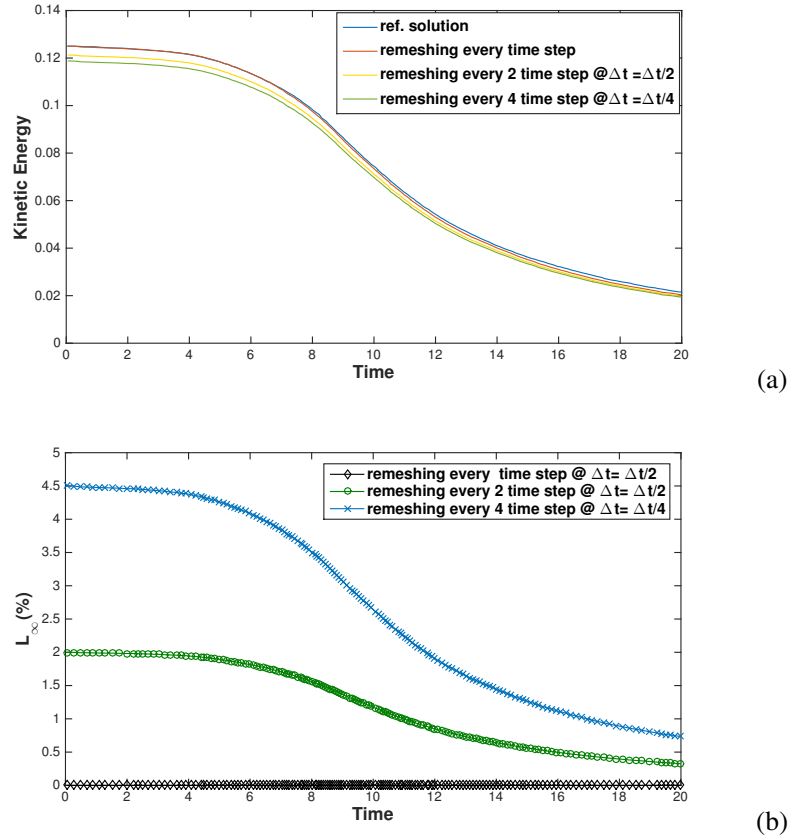


Figure 14. The effect of remeshing frequency on the the evolution of the kinetic energy for the 3D Taylor-Green simulation (a), and the relative error of remeshing every 2 and 4 time steps (b), for the simulation of the 3D Taylor-Green at $Re = 1600$.

4.4. Three-dimensional isotropic turbulence

We use hrSPH method to simulate three-dimensional isotropic turbulence in a periodic cube of size $L = 2\pi$ with a resolution of 64^3 . The initial conditions are obtained from the JHU Turbulence Database Cluster [40] a 1024^4 space-time history of a direct numerical simulation of incompressible isotropic forced turbulent flow at $Re \approx 1460$.

The data from the database contains the three velocity components and the pressure, the data is for incompressible flow. A uniform non-dimensionalised pressure $p^* = \frac{p}{\rho U^2} + 1$ is added to the database pressure, with Mach number $Ma = 0.1$. The 1024^3 resolution mesh is filtered with a Gaussian filter with a specified cutoff to reduce the noise, and then down sampled to the desired resolution (64^3).

Both the DNS and Smagorinsky models are used to predict the three-dimensional isotropic turbulence problem, the Reynolds number ranging from $Re = 300$ to 10^4 . The aim here is to study the Reynolds number threshold for both models by maintaining the same resolution.

The simulation results that the DNS fails to properly predict the turbulent flow for $Re > 2 \times 10^3$. This is caused by the insufficiently fine mesh resolution required to solve the many small scales the DNS is taking into account. The Smagorinsky model on the other hand fails with the same resolution for $Re > 6 \times 10^3$, with the same resolution (64^3).

The energy spectrum is calculated as following, for each component of the velocity fields on the grid the $u = (u_i, u_j, u_z)$ Fourier transformation is computed and denoted as $\hat{u} = (u_{ki}, u_{kj}, u_{kz})$.

The velocity spectrum tensor is computed as [41]:

$$E(\mathbf{k}) = \frac{1}{2} |\hat{u}(\mathbf{k}) \cdot \hat{u}^*(\mathbf{k})|, \quad (31)$$

where \hat{U}^* is the complex conjugate of the transform velocity, and $\mathbf{k} = (k_i, k_j, k_z)$ is the wave number. Finally the energy spectrum $E(k)$ is obtained as

$$E(k) = 4\pi k^2 \langle E(\mathbf{k}) \rangle, \quad (32)$$

where $\langle \dots \rangle$ is an average over the thin spheric shell of radius $k = |\mathbf{k}|$.

The temporal evolution of the energy spectrum for both models (DNS and Smagorinsky) with $Re = 2 \times 10^3$ is shown in Fig. 15, along with the kinetic energy evolution for both models in Fig. 16. It can be observed that the energy spectra in Fig. 15 are in good agreement. It can also be seen that more energy is dissipated by the Smagorinsky model for high wave numbers. Fig. 16 shows the subgrid model to dissipate energy faster than the DNS model due to the modelled small scales.

The Courant number (CFL) defined in Eq. (10) is an important indicator of the stability of the method, Fig. 17 shows the time evolution of the Courant number for both models at $Re = 2 \times 10^3$. It can be observed that the DNS produces high error and gradients, with big instability in the Courant number as it tries to resolve the many small scales in the turbulent flow, however the Courant number stabilised after time $t = 20$, on the other hand Smagorinsky model did not suffer of such instability and the Courant number is decreasing in relatively stable manner.

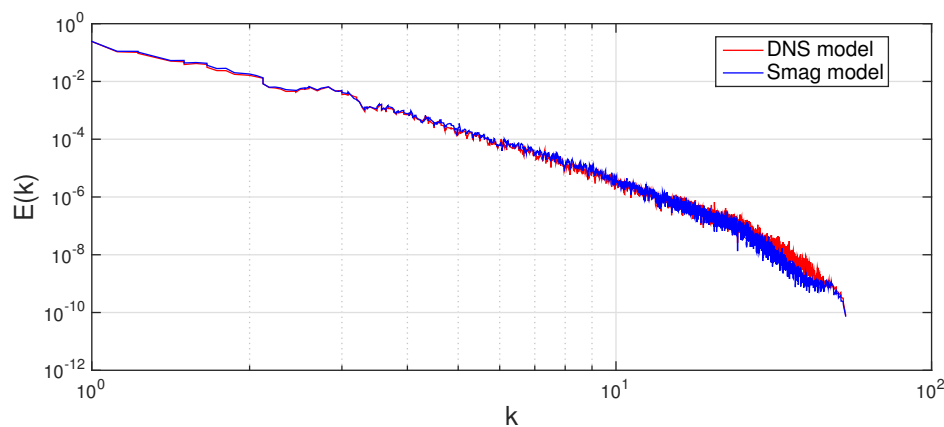


Figure 15. The energy spectra, for both the DNS and the Smagorinsky model, with $Re = 2 \times 10^3$ using the hrSPH method. It can be observed that the energy spectra are in good agreement. It can also be seen that more energy is dissipated by the Smagorinsky model for high wave numbers.

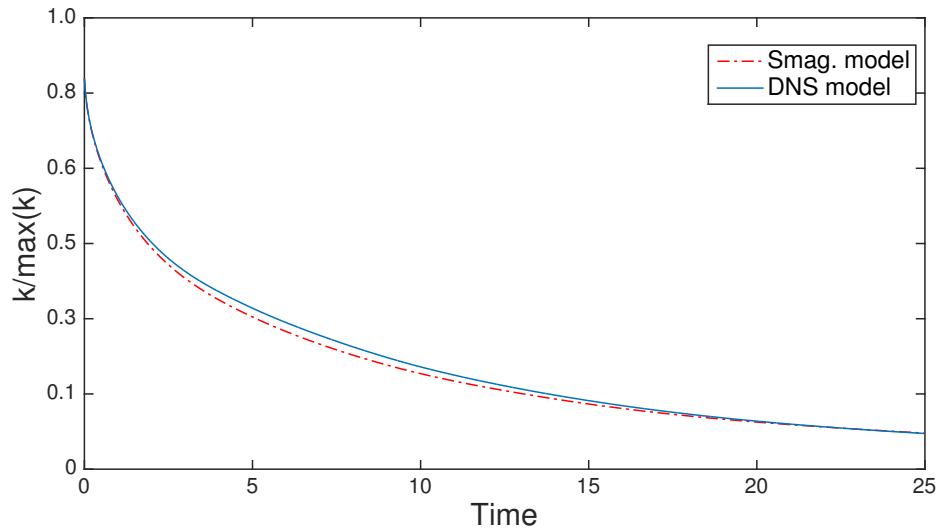


Figure 16. The kinetic energy evolution in time, evaluated for both the DNS and the Smagorinsky model, with $Re = 2 \times 10^3$ using the hrSPH method. Here the subgrid model dissipate energy faster than the DNS model due to the modelled small scales.

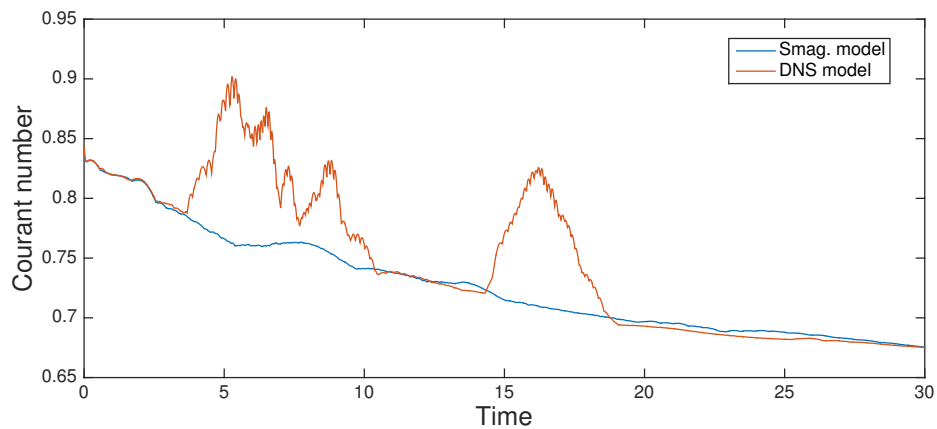


Figure 17. The Courant number evolution for the Smagorinsky and DNS model with $Re = 2 \times 10^3$. It can be observed that the DNS produces high error and gradients, with big instability in the Courant number as it tries to resolve the many small scales in the turbulent flow

Fig. 18 (a) shows the initialised velocity at time $t = 0$ and the simulated velocity magnitude decay Fig. 18 (b),(c), and (d) for Reynolds number $Re = 6 \times 10^3$. The hrSPH method with Smagorinsky model is used with remeshing every time step, as we find that for flow with strong vorticity the particle distribution becomes distorted and the particles tend to clustered so that remeshing in each time step is necessary.

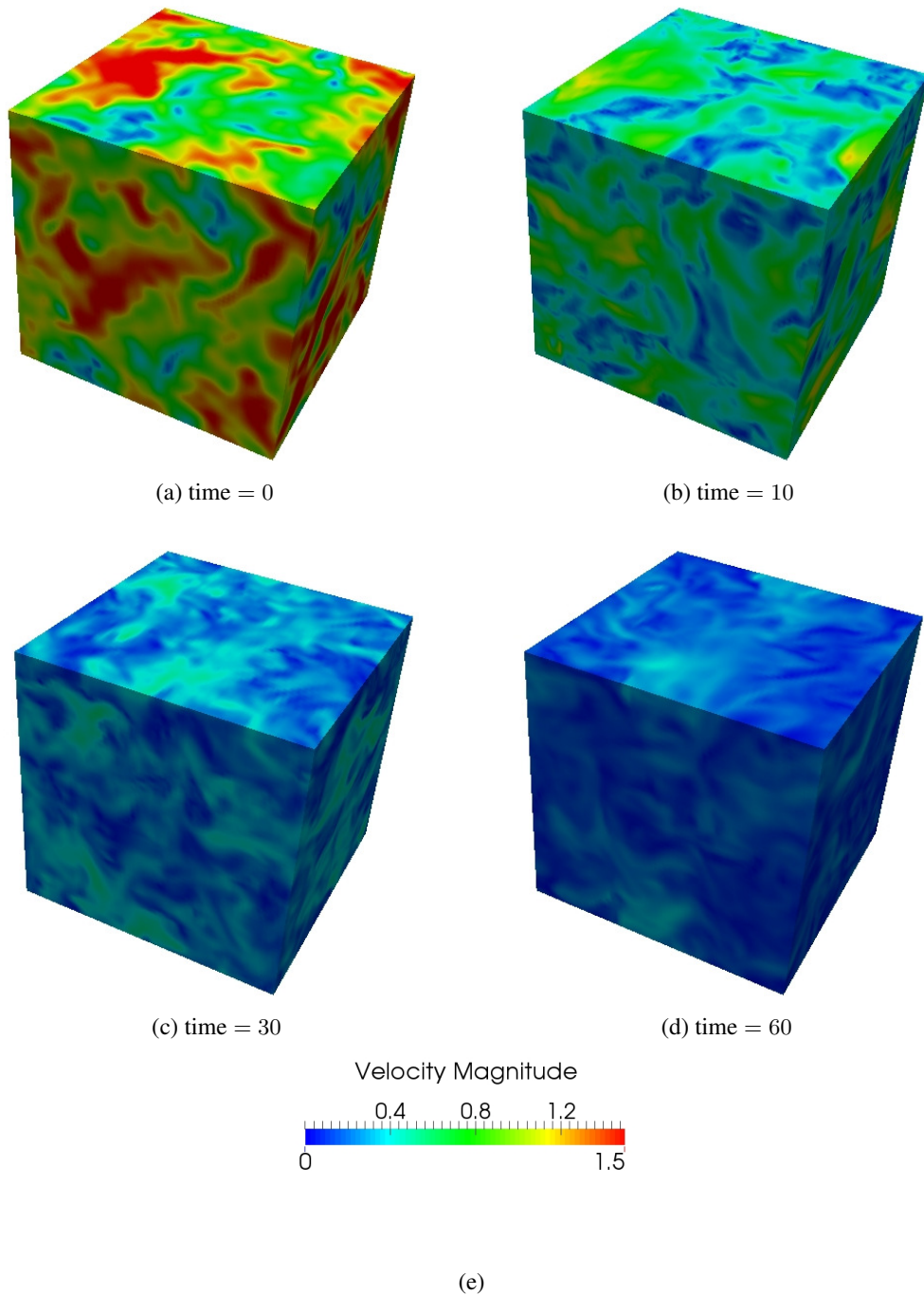


Figure 18. Velocity magnitude decay of the isotropic turbulence case

The energy spectrum calculated as in Eq. (31), and the dissipation of the energy agrees with the Kolmogorov $-5/3$ profile [25]. The temporal evolution of the energy spectrum from the initial state to the stationary state at time= 60 is shown in Fig. 19.

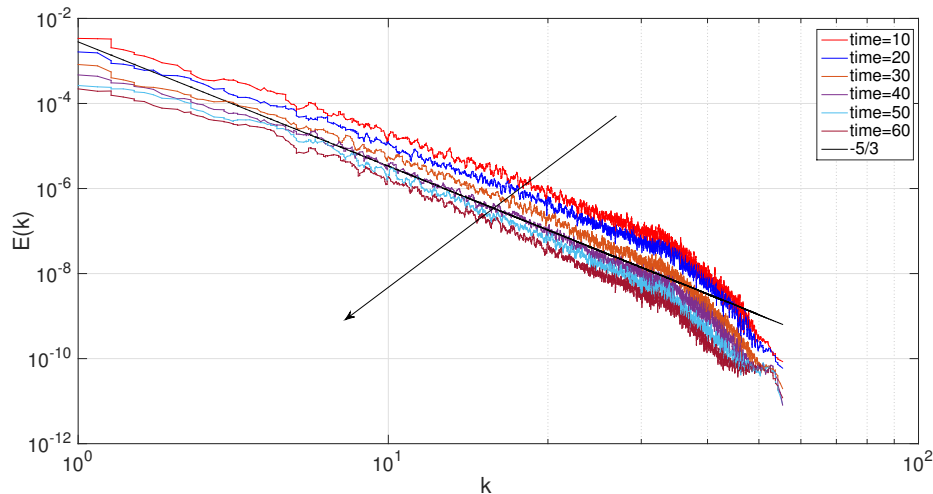


Figure 19. Time evolution of the energy spectra, evaluated at different time during the simulation, $Re = 6 \times 10^3$ using the hrSPH method with Smagorinsky mode, along with the Kolmogorov $-5/3$ profile.

5. CONCLUSION

We presented a hybrid remeshed smoothed particle hydrodynamics method (hrSPH), taking advantage of the Lagrangian advection, and the finite difference efficiency by computing the differential operators on the mesh.

Two models were used a DNS model, and a Smagorinsky model. We verified our method through several benchmarks, the hrSPH is able to resolve the flow with varying Reynolds number from 1 up to 10^4 . The method showed a third order converging for the Taylor Green flow case.

As a result of the Lagrangian advection that the method enjoys, we were able to resolve the double thin shear layer without producing the spurious vortical structure with a coarser mesh than what other studies suggested. And finally, the hrSPH method resolved the three-dimensional isotropic turbulence flow with high Reynolds number on a coarse mesh using Smagorinsky model.

6. ACKNOWLEDGEMENTS

The author is grateful to the European Research Council for the European Research Council Starting Independent Research Grant (ERC Stg grant agreement No. 279578) entitled "Towards real time multiscale simulation of cutting in non-linear materials with applications to surgical simulation and computer guided surgery" for their finance support to the project. We also thank the funding from the Luxembourg National Research Fund (INTER/MOBILITY/14/8813215/CBM/Bordas).

The authors also acknowledge the support of the Computational Science Research Priority at the University of Luxembourg. John Hopkins University (JHU) Turbulence Database Cluster, for their raw turbulence data that are used in our simulation. Professor Jens H. Walther from Denmark Technical University, for their helpful discussions and supervision. This work was performed using the computational facilities of the Advanced Research Computing@Cardiff (ARCCA) Division, Cardiff University, also this paper were carried out using the HPC facilities of the University of Luxembourg

REFERENCES

1. Dalrymple R. A. and Rogers B. D. Numerical modeling of water waves with the SPH method. *Coastal Engng.*, 53:141–147, 2006.

2. Gingold R. A. and Monaghan J. J. Smoothed particle hydrodynamics: theory and application to non-spherical stars. *MONTH Notices Roy. Astron. Soc.*, 181:375–389, 1977.
3. Milton A. and Stegun I. *Handbook of Mathematical Functions With Formulas, Graphs and Mathematical Tables*. National Bureau of Standards. Applied Mathematics Series. 55, 1972.
4. Lucy L. B. A numerical approach to the testing of the fission hypothesis. *Astron. J.*, 82:1013–1024, 1977.
5. Pope S. B. A more general effective-viscosity hypothesis. *J. Fluid Mech.*, 72(2):331–340, 1975.
6. Drikakis D. and Smolarkiewicz P. K. On spurious vortical structures. *J. Comput. Phys.*, 172:309–325, 2001.
7. Rossinelli D. and Koumoutsakos P. Vortex methods for incompressible flow simulations on the GPU. *Visual Comput.*, 24:699–708, 2008.
8. Violeau D. and Issa R. Numerical modelling of complex turbulent free-surface flows with the SPH method: an overview. *Int. J. Numer. Meth. Fluids*, 53(2):277–304, 2007.
9. Cottet G-H. and Koumoutsakos P. *Vortex Methods – Theory and Practice*. Cambridge University Press, New York, 2000.
10. Takeda H., Miyama S. M., and Sekiya M. Numerical simulation of viscous flow by smoothed particle hydrodynamics. *Prog. Theor. Phys.*, 92(5):939–960, 1994.
11. Taylor G. I. and Green A. E. Mechanism of the Production of Small Eddies from large ones. *Proc. R. Soc. Lond.*, 158(893):499–521, 1937.
12. Cummins S. J. and Rudman M. An SPH projection method. *J. Comput. Phys.*, 152(2):584–607, 1999.
13. Mansour J. *SPH and α -SPH: Applications and Analysis*. PhD. thesis, Monash University, October 2007.
14. Monaghan J. J. Particle methods for hydrodynamics. *Comput. Phys. Rep.*, 3:71–123, 1985.
15. Monaghan J. J. Simulating free surface flows with SPH. *J. Comput. Phys.*, 110:399–406, 1994.
16. Monaghan J. J. SPH compressible turbulence. *Mon. Not. R. Astron. Soc.*, 335:843–852, 2002.
17. Smagorinsky J. General circulation experiments with the primitive equations, part I: the basic experiment. *Monthly Weather Rev.*, 91(3):99–164, 1963.
18. Stam J and Fiume E. Depicting fire and other gaseous phenomena using diffusion processes. *Proceedings of the 22nd Annual Conference on Computer Graphics and Interactive Techniques*, pages 129–136, 1995.
19. Watkins S. J., Bhattal A. S., Francis N., Turner J. A., and Whitworth A. P. A new prescription for viscosity in smoothed particle hydrodynamics. *A & A S*, 119:177–187, 1996.
20. Chaniotis A. K., Poulidakos D., and Koumoutsakos P. Remeshed smoothed particle hydrodynamics for the simulation of viscous and heat conducting flows. *J. Comput. Phys.*, 182(1):67–90, 2002.
21. Minion M. L. and Brown D. L. Performance of under-resolved two-dimensional incompressible flow simulations, II. *J. Comput. Phys.*, 138:734–765, 1997.
22. Ellero M., Español P., and Adams N. A. Implicit atomistic viscosities in smoothed particle hydrodynamics. *Phys. Rev. E*, 82:046702, 2010.
23. Müller M., Charypar D., and Gross M. Particle-Based Fluid Simulation for Interactive Applications. *Proceedings of the 2003 ACM SIGGRAPH/Eurographics symposium on Computer animation*, pages 154–159, 2003.
24. Robinson M. and Monaghan J. J. Direct numerical simulation of decaying two-dimensional turbulence in a no-slip square box using smoothed particle hydrodynamics. *Int. J. Numer. Meth. Fluids*, 70(1):37–55, 2012.
25. Kolmogorov A. N. The Local Structure of Turbulence in Incompressible Viscous Fluid for Very Large Reynolds Numbers. *Dokl. Akad. Nauk SSSR*, 30:301–305, 1941.
26. Chatelain P., Cottet G.-H., and Koumoutsakos P. PMH: Particle-mesh hydrodynamics. *Int. J. Mod. Phys. C*, 18(4):610–618, 2007.
27. Koumoutsakos P. *Direct Numerical Simulations of Unsteady Separated Flows Using Vortex Methods*. Ph.d. thesis, California Institute of Technology, 1993.
28. Koumoutsakos P. Inviscid axisymmetrization of an elliptical vortex ring. *J. Comput. Phys.*, 138:821–857, 1997.
29. Koumoutsakos P. Multiscale flow simulations using particles. *Annu. Rev. Fluid Mech.*, 37:457–487, 2005.
30. Koumoutsakos P. and Leonard A. High-resolution simulation of the flow around an impulsively started cylinder using vortex methods. *J. Fluid Mech.*, 296:1–38, 1995.
31. Morris J. P. Simulating surface tension with smoothed particle hydrodynamics. *Int. J. Numer. Meth. Fluids*, 33(3):333–353, 2000.
32. Morris J. P., Fox P. J., and Zhu Y. Modeling low Reynolds number incompressible flows using SPH. *J. Comput. Phys.*, 136:214–226, 1997.
33. Adami S., Hu X. Y., and Adams N. A. A transport-velocity formulation for smoothed particle hydrodynamics. *J. Comput. Phys.*, 241:292–307, 2013.
34. Rogallo R. S. and Moin P. Numerical simulation of turbulent flows. *Annu. Rev. Fluid Mech.*, 16:99–137, 1984.
35. Shao S. and Lo E. Y. M. Incompressible SPH method for simulating Newtonian and non-Newtonian flows with a free surface. *Adv. Water Res.*, 26:787–800, 2003.
36. I. A. Shirokov and T. G. Elizarova. Simulation of laminar-turbulent transition in compressible Taylor-Green flow basing on quasi-gas dynamic equations. *Journal of Turbulence*, 15(10):707–730, 2014.
37. Rees W. M. van, Leonard A., Pullin D. I., and Koumoutsakos P. A comparison of vortex and pseudo-spectral methods for the simulation of periodic vortical flows at high Reynolds numbers. *J. Comput. Phys.*, 230:2794–2805, 2011.
38. Cleary P. W. and Monaghan J. J. Conduction modelling using smoothed particle hydrodynamics. *J. Comput. Phys.*, 148:227–264, 1999.
39. Hockney R. W. and Eastwood J. W. *Computer Simulation Using Particles*. Institute of Physics Publishing, Bristol, PA, USA, 2. edition, 1988.
40. Li Y., Perlman E., Wan M., Yang Y., Meneveau C., Burns R., Chen S., Szalay A., and Eyink G. A public turbulence database cluster and applications to study Lagrangian evolution of velocity increments in turbulence. *J. of Turbomachinery*, 9(31):1–29, 2008.
41. Shi Y., Ellero M., and Adams N. A. Analysis of intermittency in under-resolved smoothed-particle-hydrodynamics direct numerical simulations of forced compressible turbulence. *Phys. Rev. E*, 85:036708, 2012.